Contribution from the Department of Chemistry,
University of Houston, Houston, Texas 77004

Electrochemistry of (Tetraphenylporphinato)rhodium(III) Alkyl and Alkyl Halide Complexes. Effect of the σ-Bonded Ligand on Porphyrin Reactivity

J. E. Anderson, Y. H. Liu, and K. M. Kadish*

Received March 17, 1987

The electrochemistry of 17 different (tetraphenylporphinato)rhodium(III) complexes of the form (TPP)Rh(R) and (TPP)Rh(RX) are reported, where TPP is the dianion of tetraphenylporphyrin, R = C_6H_5 or C_nH_{2n+1} (n = 1-6), and RX = $C_nH_{2n}Cl$ (n = 3-5), $C_nH_{2n}Br$ (n = 3-5), or $C_nH_{2n}I$ (n = 3-6). The nature of the R or RX group determines the overall electrochemical behavior for the reduction of (P)Rh(R) or (P)Rh(RX). For some complexes the bound alkyl halide can be reduced without cleavage of the metal-carbon bond, and this results in the electrochemically initiated conversion of (TPP)Rh(RX) to a (TPP)Rh(R) complex. A general reduction scheme is presented that summarizes the electrochemistry of these compounds.

Introduction

Electrochemical properties of monomeric and dimeric rhodium porphyrins of the type $[(TPP)Rh(L)_2]^+Cl^-$, (TPP)Rh(L)(Cl), and $[(TPP)Rh]_2$ have been reported,[1] where TPP is the dianion of tetraphenylporphyrin and L is dimethylamine. Oxidation of the monomeric Rh(III) complex occurs at the porphyrin π ring system while reduction of the complex occurs at the metal center. This Rh(III)/Rh(II) reaction is followed by one of two types of chemical reactions. One involves formation of a σ-bonded Rh(III) complex while the other involves dimerization of (TPP)Rh to give $[(TPP)Rh]_2$. These competing reaction pathways of (TPP)Rh are summarized in Scheme I. The electrochemical properties of $[(TPP)Rh]_2$ and (TPP)Rh(R) synthesized via these pathways have been reported[1,2] and compared to properties of (TPP)Rh-$(COCH_3)$.[3]

In this paper we report the synthesis and electrochemical properties of different rhodium(III) porphyrins containing σ-bonded alkyl halides. The synthesis of these rhodium porphyrins σ-bonded to alkyl halides has not been previously reported and provides a series of compounds where the electrochemical reduction may occur at the porphyrin π ring system, at the central Rh(III) ion, or at the complexed alkyl halide. Seventeen different complexes are investigated in this study. These include (TPP)Rh(R), where R = C_nH_{2n+1} (n = 1-6) or C_6H_5, and (TPP)Rh(RX), where RX = $C_nH_{2n}Cl$ (n = 3-5), $C_nH_{2n}Br$ (n = 3-5), or $C_nH_{2n}I$ (n = 3-6). In all cases the R or RX group is the straight-chain isomer and for RX, the halide is on the CH_2 group farthest from the Rh center.

A generally accepted mechanism for reduction of free RX in nonaqueous media is shown by eq 1-3.[4,5] This study demonstrates

$$RX + e^- \rightarrow RX^- \quad (1)$$

$$RX^- \rightarrow R^\bullet + X^- \quad (2)$$

$$R^\bullet + e^- \rightarrow R^- \quad (3)$$

that a similar reduction of the bound alkyl halide on (TPP)Rh-(RX) is possible without cleavage of the Rh-carbon bond and that this reduction occurs at potentials significantly positive of those for reduction of free RX. Also, the results of this study clearly demonstrate that the nature of the R or RX group of (TPP)Rh(R) and (TPP)Rh(RX) can determine the overall electrochemical behavior for reduction.

Scheme I

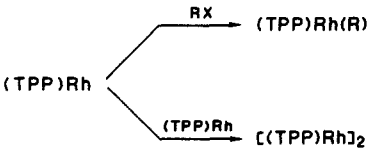

Experimental Section

Instrumentation and Methods. An IBM 225/2A voltammetric analyzer and a Houston Instruments Model 2000 X-Y recorder were used for cyclic voltammetric measurements. Thin-layer spectroelectrochemical measurements were performed with an IBM 225/2A voltammetric analyzer coupled with a Tracor Northern 1710 spectrometer/multichannel analyzer. Bulk controlled-potential coulometry was performed on an EG&G Princeton Applied Research Model 174 potentiostat/179 coulometer system, coupled with an EG&G Princeton Applied Research Model RE-0074 time base X-Y recorder. Cells used for bulk electrolysis experiments were modified for Schlenk techniques. Platinum-disk electrodes were used for cyclic voltammetric measurements, and platinum-minigrid electrodes were used in both the thin-layer spectroelectrochemical cell and the bulk electrolysis cell. The thin-layer spectroelectrochemical cell has been previously described.[6] Potentials were measured vs a saturated calomel electrode (SCE) separated from the bulk of the solution by a fritted-glass disk junction. The ferrocene/ferrocenium couple was used as an internal standard against which potentials were also measured. Unless otherwise noted, 0.2 M tetrabutylammonium (TBAP) was used as supporting electrolyte in all electrochemical and spectroelectrochemical experiments.

UV-visible spectra were measured either on a Tracor Northern 1710 spectrometer/multichannel analyzer or with an IBM 9430 spectrophotometer using cells adapted for inert-atmosphere measurements. NMR spectra were measured on a Nicolet FT 300 spectrometer. Gas chromatographic analysis was performed with a Hewlett Packard 5890 gas chromatograph coupled with a Hewlett Packard 3392A integrator.

Materials. Reagent grade benzonitrile (PhCN) was predried with Na_2CO_3 and then vacuum distilled over P_2O_5 prior to use. Spectroscopic grade tetrahydrofuran (THF) was purchased from Aldrich and purified by distillation under nitrogen first from CaH_2 and then from Na/benzophenone just prior to use. Tetra-*n*-butylammonium perchlorate (TBAP) was purchased from Fluka Chemical Co., twice recrystallized from ethyl alcohol, and dried in a vacuum oven at 40 °C. All organic reagents (Aldrich) were purchased at the highest level of purity available, purified by standard procedures[7] where necessary, and checked for impurities by gas chromatographic analysis. Deuteriated benzene-d_6 (C_6D_6) was purchased from Aldrich and used without further purification.

Synthesis of (TPP)Rh(R). (TPP)Rh(C_6H_5), (TPP)Rh(CH_3), and $[(TPP)Rh(L)_2]^+Cl^-$, where L is dimethylamine, were synthesized by literature methods.[1,8-10] The other (TPP)Rh(R) and (TPP)Rh(RX)

(1) Kadish, K. M.; Yao, C.-L.; Anderson, J. E.; Cocolios, P. *Inorg. Chem.* **1985**, *24*, 4515.
(2) Anderson J. E.; Yao, C.-L.; Kadish, K. M. *J. Am. Chem. Soc.* **1987**, *109*, 1106.
(3) Kadish, K. M.; Anderson, J. E.; Yao, C.-L.; Guilard, R. *Inorg. Chem.* **1986**, *25*, 1277.
(4) Rifi, M. R. In *Organic Electrochemistry*; Baizen, C. C., Ed.; Marcel Dekker: New York, **1973**; p 279.
(5) Mann, C. K.; Barnes, K. K. *Electrochemical Reactions in Nonaqueous Systems*; Marcel Dekker: New York, 1970; p 201.
(6) Lin, X. Q.; Kadish, K. M. *Anal. Chem.* **1985**, *57*, 1498.
(7) Perrin, D. D.; Armarego, W. L.; Perrin, D. R. *Purification of Laboratory Chemicals*, 2nd ed.; Pergamon: New York, 1980.
(8) Hughes, R. P. In *Comprehensive Organometallic Chemistry*; Wilkinson, G., Ed.; Pergamon: New York, 1982; Vol. 5, p 388.
(9) Fleischer, E. B.; Dixon, F. L.; Florian, R. *Inorg. Nucl. Chem. Lett.* **1973**, *9*, 1303.
(10) Ogoshi, H.; Setsune, J. I.; Omura, T.; Yoshida, Z. I. *J. Am. Chem. Soc.* **1975**, *97*, 6461.

0020-1669/87/1326-4174$01.50/0

Table I. ^{1}H NMR Data for the σ-Bonded Alkyl Group of (P)Rh(R)[a]

compd	n	δ, splitting,[b] no. of H					
(TPP)Rh(C_nH_{2n+1})	1	−5.54, d, 3 H[c]					
	2	−4.61, m, 2 H	−4.19, t, 3 H				
	3	−4.65, m, 2 H	−4.10, h, 2 H	−1.77, t, 3 H			
	4	−4.60, m, 2 H	−4.18, p, 2 H	−1.57, h, 2 H	−0.81, t, 3 H		
	5	−4.63, m, 2 H	−4.18, p, 2 H	−1.62, p, 2 H	−0.51, h, 2 H	−0.27, t, 3 H	
	6	−4.61, m, 2 H	−4.16, p, 2 H	−1.56, p, 2 H	−0.53, p, 2 H	0.08, h, 2 H	0.13, t, 3 H
(TPP)Rh(C_nH_{2n}Cl)	3	−4.87, m, 2 H	−3.86, p, 2 H		0.08, 2, 2 H		
	4	−4.83, m, 2 H	−4.21, p, 2 H	−1.52, p, 2 H	1.31, t, 2 H		
	5	−4.77, m, 2 H	−4.32, p, 2 H	−1.70, p, 2 H	−0.36, p, 2 H	1.91, t, 2 H	
(TPP)Rh(C_nH_{2n}Br)	3	−4.89, m, 2 H	−3.80, p, 2 H	−0.07, t, 2 H			
	4	−4.84, m, 2 H	−4.21, p, 2 H	−1.45, p, 2 H	1.17, t, 2 H		
	5	−4.78, m, 2 H	−4.33, p, 2 H	−1.72, p, 2 H	−0.31, p, 2 H	1.74, t, 2 H	
(TPP)Rh($C_nH_{2n}I$)	3	−4.96, m, 2 H	−3.85, p, 2 H	−0.30, t, 2 H			
	4	−4.86, m, 2 H	−4.27, p, 2 H	−1.51, p, 2 H	0.89, t, 2 H		
	5	−4.79, m, 2 H	−4.35, p, 2 H	−1.76, p, 2 H	−0.35, p, 2 H	1.49, t, 2 H	
	6	−4.73, m, 2 H	−4.30, p, 2 H	−1.82, p, 2 H	−0.73, p, 2 H	0.26, p, 2 H	1.92, t, 2 H

[a] Solvent C_6D_6. [b] m = multiplet due to J_{Rh-H}; t = triplet; p = pentet; h = hextet. [c] Reference 2.

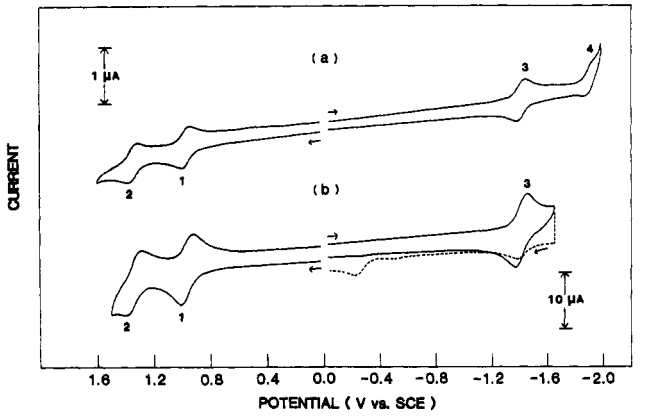

Figure 1. (a) Cyclic voltammogram of a 1.1×10^{-3} M (TPP)Rh(C_2H_5) in PhCN containing 0.2 M TBAP (scan rate = 0.1 V/s). (b) Thin-layer cyclic voltammogram of (TPP)Rh(C_2H_5) in PhCN containing 0.2 M TBAP (scan rate = 0.01 V/s): (—) first scan; (- -) reverse scan after holding for 5 min at −1.6 V.

complexes were synthesized by an electrochemical procedure similar to the one that has been previously described.[2] The identification and purity of the resulting (TPP)Rh(C_nH_{2n+1}) or (TPP)Rh(C_nH_{2n}X) complexes were determined from NMR data.

^{1}H NMR Data. ^{1}H NMR spectra for the tetraphenylporphyrin ring of (TPP)Rh(R) and (TPP)Rh(RX) can be summarized as follows: pyr-H, 8.86 ± 0.05 ppm, s, 8 H; *o*-H, 8.20 ± 0.5 ppm, m, 8 H; *m,p*-H, 7.49 ± 0.05 ppm, m, 12 H. Resonances of the σ-bonded R and RX ligand for each individual compound are summarized in Table I.

Results and Discussion

Oxidation of (TPP)Rh(R) and (TPP)Rh(RX). Each (TPP)Rh(R) and (TPP)Rh(RX) complex undergoes two reversible, diffusion-controlled one-electron oxidations by cyclic voltammetry. Both processes are characterized by $\Delta E_p = 60 \pm 5$ mV, a constant $i_p/v^{1/2}$ and $|E_p - E_{p/2}| = 60 \pm 5$ mV. This is illustrated by the voltammogram of (TPP)Rh(C_2H_5) in PhCN containing 0.1 M TBAP (Figure 1).

Similar reversible oxidative behavior was observed for all 17 investigated (TPP)Rh(R) and (TPP)Rh(RX) complexes whose oxidation potentials are listed in Table II. As seen in this table, the values of $E_{1/2}$ vary little with the nature of the σ-bonded alkyl ligand and occur at 0.98 ± 0.01 V (wave 1, Figure 1a) and 1.35 ± 0.01 V (wave 2, Figure 1a) in PhCN. The insensitivity of $E_{1/2}$ to the specific R or RX group suggests that the electron abstractions occur at the porphyrin π ring system. This site of electron abstraction is also suggested by the 0.37 ± 0.02 V difference in $E_{1/2}$ between the two oxidations in PhCN, which is close to the experimentally observed $\Delta E_{1/2}$ of 0.29 ± 0.05 V for consecutive ring oxidations of a number of metalloporphyrins.[11]

Thin-layer cyclic voltammograms of (TPP)Rh(R) and (TPP)Rh(RX), where R = C_6H_5, CH_3, C_2H_5, or C_5H_{11} and RX = $C_nH_{2n}I$ (n = 3–6), also show two reversible, one-electron oxidations on the cyclic voltammetric time scale. This is illustrated in Figure 1b for (TPP)Rh(C_2H_5) in PhCN. Thin-layer coulometric oxidation of (TPP)Rh(C_2H_5) at 1.20 V gives a calculated value of n = 1.2 ± 0.1 electrons abstracted per rhodium atom. However, bulk electrolysis of (TPP)Rh(C_2H_5) as well as other compounds in the (TPP)Rh(R) or (TPP)Rh(RX) series indicates that a chemical reaction follows the initial oxidation and n values greater than 1.0 are obtained. For example, bulk electrolysis of (TPP)Rh(C_3H_7) at 1.20 V in PhCN shows the abstraction of 2.1 ± 0.1 electrons. This suggests a cleavage of the Rh–carbon bond and further oxidation of the generated [(TPP)Rh]$^+$ species.

Changes in the electronic absorption spectrum of (TPP)Rh(C_2H_5) as the compound is oxidized at 1.20 V vs SCE in PhCN

Table II. Oxidation and Reduction Potentials (V vs SCE) for (TPP)Rh(R)

R group	solvent	temp, °C	oxidn		redn		
CH_3	THF	23			−1.45		−1.90
C_2H_5	THF	23	1.12		−1.41		−1.90
	PhCN	23	0.97	1.35	−1.41		−1.90
C_3H_7	THF	23			−1.42		−1.91
	PhCN	23	0.97	1.33	−1.40		−1.89
C_4H_9	THF	23			−1.42		−1.92
	PhCN	23	0.97	1.34	−1.41		−1.90
C_5H_{11}	THF	23			−1.42		−1.91
	PhCN	23	0.98	1.34	−1.40		−1.89
C_6H_{13}	THF	23			−1.42		−1.91
	PhCN	23	0.97	1.34	−1.41		−1.90
C_6H_5	THF	23			−1.40		−1.81
	PhCN	23	0.99	1.38	−1.39		−1.84
C_3H_6Cl	THF	23	1.17		−1.41		−1.86
C_4H_8Cl	THF	23	1.14		−1.41		−1.88
$C_5H_{10}Cl$	THF	23	1.14		−1.42		−1.90
C_3H_6Br	THF	23			−1.39	−1.81[a]	−1.83[b]
	THF	−75	1.11	1.32	−1.42		−1.88
C_4H_8Br	THF	23	1.14		−1.40	−1.85[a]	−2.01[a]
	THF	−70	1.10	1.33	−1.44		−1.87
$C_5H_{10}Br$	THF	23	1.14		−1.40		−1.89[a]
	THF	−74	1.10	1.34	−1.44		−1.88
C_3H_6I	THF	23	1.15		−1.38[a]		−1.83[b]
	THF	−70	1.13	1.34	−1.43		−1.88[a]
	PhCN	23	0.98	1.35	−1.37[a]		−1.84
C_4H_8I	THF	23	1.15		−1.39	−1.78[a]	−1.99[a]
	THF	−75	1.09	1.33	−1.42	−1.86[a]	−2.07
	PhCN	23	0.97	1.34	−1.41		−1.92[a]
$C_5H_{10}I$	THF	23	1.15		−1.40	−1.81[a]	−1.88
	THF	−76	1.10	1.33	−1.43		−1.90[a]
	PhCN	23	0.98	1.35	−1.41	−1.86[a]	−1.89
$C_6H_{12}I$	THF	23	1.14		−1.41	−1.82[a]	−1.88
	THF	−76	1.10	1.34	−1.44		−1.94[a]
	PhCN	23	0.99	1.35	−1.40		−1.89

[a] E_p, scan rate = 100 mV/s, process 5; see text. [b] Due to reduction of [(TPP)Rh]$_2$; see ref 1.

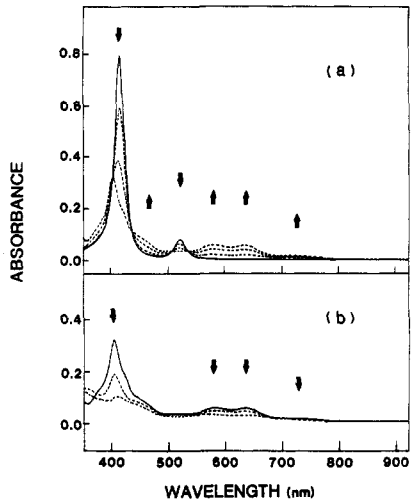

Figure 2. Electronic absorption spectra of (a) neutral and singly oxidized (TPP)Rh(C_2H_5) and (b) singly and doubly oxidized (TPP)Rh(C_2H_5) in PhCN containing 0.2 M TBAP.

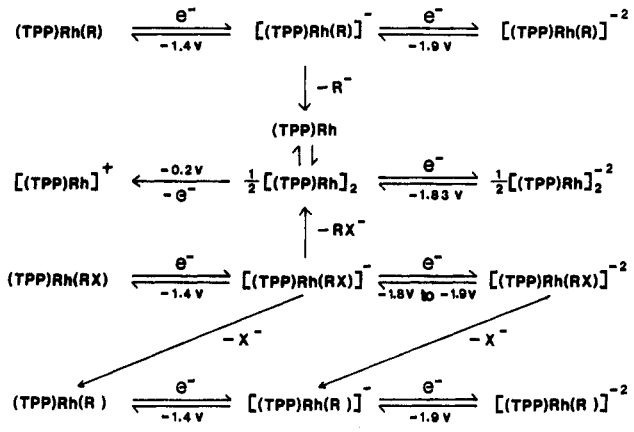

Figure 3. Reaction scheme for the electroreduction of (TPP)Rh(R) and (TPP)Rh(RX) in THF.

are shown in Figure 2a. As the oxidation proceeds, the Soret band, which is initially at 416 nm, decreases in intensity and shifts to 403 nm. The absorption band at 522 nm also decreases in intensity as new bands are observed at 585 and 640 nm. These changes in the UV–visible spectrum indicate electron abstraction from a porphyrin ring based orbital with formation of a cation radical.[11]

The electrooxidation of (TPP)Rh(C_2H_5) is not reversible, and the original spectrum is not regenerated when the potential is reset to 0.70 V. This type of irreversibility upon electrooxidation was observed for the other (TPP)Rh(R) and (TPP)Rh(RX) compounds. In all cases, a chemical reaction followed the initial oxidation, but for most complexes the rate of this reaction was relatively slow and reversible cyclic voltammetric behavior was obtained.

Figure 2b shows representative changes that occur in the UV–visible spectrum of (TPP)Rh(C_2H_5) upon switching the potential from 1.20 to 1.50 V. The Soret band continues to decrease in intensity during the second oxidation. There is also a general decrease in intensity of the Q bands, typical of dication formation.[11] This oxidation is also not reversible, and the original spectrum is not regenerated if the potential is set back to 0.70 V. Similar UV–visible spectral changes are obtained during the second oxidation of each (TPP)Rh(R) and (TPP)Rh(RX) complex investigated. Thus spectroelectroelectrochemical results confirm that the initial oxidations of (TPP)Rh(R) and (TPP)Rh(RX) occur at the porphyrin π ring system but also indicate that the singly and doubly oxidized species are involved in a chemical reaction. A complete summary of the spectroelectrochemical data for the oxidation of each (TPP)Rh(R) and (TPP)Rh(RX) complex before the chemical reaction occurs is presented in Table III.

(11) Kadish, K. M. *Prog. Inorg. Chem.* **1986**, *34*, 435.

Table III. UV–Visible Spectra of Complexes in PhCN Containing 0.2 M TBAP

complex	R group	solvent	λ_{max}, nm ($\epsilon \times 10^{-4}$)		
(TPP)Rh(R)	CH_3	PhCN	418 (22.9)	525 (2.3)	
	C_2H_5	THF	411 (21.6)	524 (1.9)	
		PhCN	416 (21.3)	522 (2.2)	
	C_3H_7	THF	411 (17.7)	524 (1.5)	
	C_4H_9	THF	411 (21.5)	524 (1.7)	
	C_5H_{11}	THF	411 (25.2)	524 (2.3)	
		PhCN	416 (20.1)	522 (2.3)	
	C_6H_{13}	THF	411 (27.9)	524 (2.8)	
	C_6H_5	THF	413 (20.8)	525 (2.2)	
(TPP)Rh(RX)	C_3H_6Cl	THF	411 (27.2)	524 (2.5)	
	C_4H_8Cl	THF	411 (27.9)	524 (2.7)	
	$C_5H_{10}Cl$	THF	411 (24.9)	524 (2.0)	
	C_3H_6Br	THF	411 (24.7)	524 (2.4)	
	C_4H_8Br	THF	411 (29.2)	524 (3.2)	
	$C_5H_{10}Br$	THF	411 (23.7)	524 (1.9)	
	C_3H_6I	THF	411 (26.9)	524 (2.2)	
		PhCN	417 (21.9)	524 (2.2)	
	C_4H_8I	THF	411 (30.9)	524 (2.6)	
	$C_5H_{10}I$	THF	411 (27.7)	524 (2.2)	
	$C_6H_{12}I$	THF	411 (27.2)	524 (2.2)	
$[(TPP)Rh(R)]^+$	CH_3	PhCN	404 (8.8)	583 (1.6)	645 (1.4)
	C_2H_5	PhCN	403 (8.7)	585 (1.5)	640 (1.4)
	C_5H_{11}	PhCN	403 (8.6)	579 (1.5)	639 (1.4)
$[(TPP)Rh(RX)]^+$	C_3H_6I	PhCN	405 (9.7)	583 (1.7)	539 (1.5)
$[(TPP)Rh(R)]^{2+}$	CH_3	PhCN	413 (3.4)	564 (0.8)	645 (0.7)
	C_2H_5	PhCN	411 (2.6)	566 (0.8)	640 (0.6)
	C_5H_{11}	PhCN	408 (3.9)	566 (1.1)	651 (0.7)
$[(TPP)Rh(RX)]^{2+}$	C_3H_6I	PhCN	408 (4.8)	562 (1.0)	654 (0.6)

Reduction Pathways of (TPP)Rh(R) and (TPP)Rh(RX). Figure 3 summarizes the overall electrochemical and chemical reaction pathways that can occur upon reduction of different (TPP)Rh(R) and (TPP)Rh(RX) complexes. The specific group of compounds that follow a given reduction pathway can be divided into two sets. The first set of compounds is comprised of (TPP)Rh(R), where R = C_nH_{2n+1} (n = 1–6) or C_6H_5, and (TPP)Rh(RX), where RX = $C_nH_{2n}Cl$ (n = 3–5). These metalloporphyrins can undergo two reversible ring reductions (at −1.4 and −1.9 V), but the singly reduced species undergo a cleavage of the Rh–carbon bond on longer time scales.

The second set of compounds is comprised of (TPP)Rh(RX), where RX = $C_nH_{2n}Br$ (n = 3–5) or $C_nH_{2n}I$ (n = 3–6). For these compounds an important intermediate in the electrochemistry is the $[(TPP)Rh(RX)]^-$ monoanion. This species can lose X^-, lose RX^-, or be further reduced at the axial ligand. The particular pathway for reaction of (TPP)Rh(RX) depends upon the individual RX species and the given reaction conditions such as temperature or scan rate. These pathways are given by the overall reactions 4 and 5 and are discussed in the following sections.

$$(TPP)Rh(RX) + 2e^- \rightarrow [(TPP)Rh(R)]^- + X^- \quad (4)$$

$$(TPP)Rh(RX) + 3e^- \rightarrow [(TPP)Rh(R)]^{2-} + X^- \quad (5)$$

Reversible Reductions of (TPP)Rh(R) and (TPP)Rh(RX), Where RX = $C_nH_{2n}Cl$ (n = 3–5). (TPP)Rh(R) and (TPP)Rh(RX), where RX = $C_nH_{2n}Cl$ (n = 3–5), undergo two reversible reductions at the porphyrin π ring system. The electrochemical behavior of these complexes is typified by (TPP)Rh(C_2H_5) in which two reversible, one-electron, diffusion-controlled reductions are observed on the cyclic voltammetric time scale. These reductions occur at $E_{1/2}$ = −1.41 and $E_{1/2}$ = −1.90 V and are labeled as waves 3 and 4 in Figure 1a. For both processes, ΔE_p = 60 ± 5 mV, $|E_p - E_{p/2}|$ = 60 ± 5 mV and $i_p/v^{1/2}$ is a constant. Similar diffusion-controlled reductions are obtained in THF.

Thin-layer cyclic voltammograms of (TPP)Rh(C_2H_5) (Figure 1b) also suggest reversible electrochemical processes, and thin-layer coulometric values for the reduction of (TPP)Rh(C_2H_5) at −1.62 V give values of n = 1.2 ± 0.1. However, decomposition of reduced (TPP)Rh(C_2H_5) and formation of $[(TPP)Rh]_2$ occurs when the potential is held at potentials negative of the first reduction for

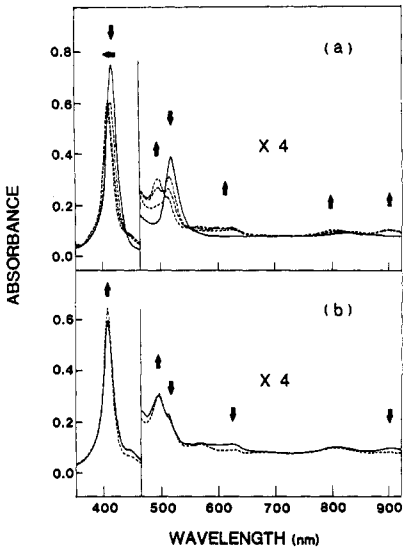

Figure 4. Electronic absorption spectra (a) during the initial reduction of (TPP)Rh(C_2H_5) at −1.6 V in PhCN containing 0.2 M TBAP and (b) after holding the reduction potential at −1.6 V for 5 min.

5 min. Dimer formation is indicated by the presence of an oxidation peak at E_p = −0.2 V (see dotted line, Figure 1b).[1]

Figure 4a shows changes that occur in the UV–visible spectra of (TPP)Rh(C_2H_5) upon reduction at −1.65 V in PhCN. As the reduction proceeds, the Soret band is reduced in intensity and shifts to 407 nm. The Q bands also show a decrease in intensity and shift to 497 and 516 nm. New absorption bands are observed at 814 and 908 nm and are indicative of anion radical formation.[11] The original spectrum can be obtained if the potential is immediately reset to 0.0 V, but there is evidence of a chemical reaction involving the anion radical.

Spectral changes associated with porphyrin dianion formation are initially observed when the compound is reduced at −1.94 V. However, the final UV–visible spectrum has bands at 447 and 807 nm and is close to that of the product formed after decomposition of the dianion. In addition, when the potential is set back to 0.00 V, the original species is not regenerated, thus suggesting a more rapid chemical reaction of the dianion.

Figure 4b spectrally demonstrates the conversion of [(TPP)Rh(C_2H_5)]$^-$ to [(TPP)Rh]$_2$. This was accomplished by reducing (TPP)Rh(C_2H_5) at −1.65 V and holding the potential for 5 min. The final electronic absorption spectra is characterized by bands at 407, 497, and 516 nm and is indicative of [(TPP)Rh]$_2$ in PhCN solution.

Similar reductive properties are observed for (TPP)Rh(R), where R = C_nH_{2n+1} (n = 1–6) or C_6H_5 and RX = $C_nH_{2n}Cl$ (n = 3–5). Reduction potentials for this set of compounds are listed in Table II and suggest that the successive addition of one and two electrons occur at the porphyrin π ring system. The separation of 0.50 ± 0.05 V between $E_{1/2}$ values for the two reductions agrees with the $\Delta E_{1/2}$ = 0.44 ± 0.04 V generally observed for the two successive one-electron ring reductions of numerous metalloporphyrins.[11]

Spectroelectrochemical data for the reduction of (TPP)Rh(C_nH_{2n+1}) and (TPP)Rh($C_nH_{2n}Cl$) demonstrates that the initial reduction is ring centered. In most cases the anion radicals are not stable, and cleavage of the rhodium–carbon bond occurs with formation of [(TPP)Rh]$_2$. The rate of the following chemical reaction is dependent upon the R group. A relatively stable anion radical is observed for (TPP)Rh(C_6H_5) and (TPP)Rh($COCH_3$)[3] on the spectroelectrochemical time scale.

Reduction of (TPP)Rh($C_nH_{2n}I$). The reduction of (TPP)Rh(C_3H_6I) is irreversible by cyclic voltammetry in PhCN (see Figure 5a). The first reduction occurs at E_p = −1.37 V (peak 3, Figure 5a) and is shifted by +40 mV relative to $E_{1/2}$ for the first reduction of (TPP)Rh(C_2H_5). Normal pulse polarograms have twice the reduction current as the first one-electron oxidation. This is shown in Figure 5b and suggests an overall two-electron reduction of

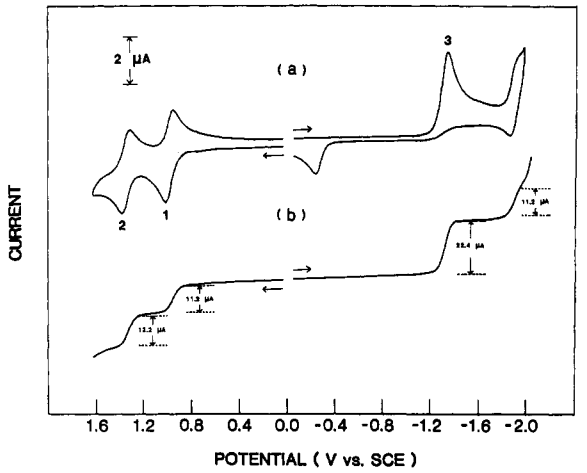

Figure 5. (a) Cyclic voltammogram and (b) normal-pulse voltammogram of (TPP)Rh(C_3H_6I) in PhCN containing 0.2 M TBAP.

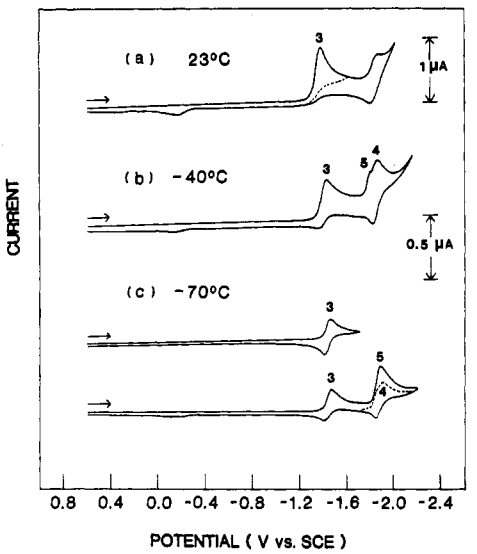

Figure 6. Cyclic voltammogram of 1.3 × 10^{-3} M (TPP)Rh(C_3H_6I) in THF containing 0.2 M TBAP at (a) 23, (b) −40, and (c) −70 °C: (—) single scan; (--) single scan with reversal of potential and second scan between −1.7 and −2.2 V (dashed line).

(TPP)Rh(C_3H_6I) in the first process. This was confirmed by thin-layer coulometry, which gave a value of n = 2.2 ± 0.2 for controlled potential reduction at −1.62 V in THF.

An additional electroreduction is also observed at $E_{1/2}$ = −1.84 V, and there is an irreversible oxidation at E_p = −0.20 V in the cyclic voltammogram. These two processes are due to [(TPP)Rh]$_2$, which is generated as a product of the chemical reaction following electroreduction.[1] The formation of [(TPP)Rh]$_2$ and I^- was detected by thin-layer voltammetric experiments on (TPP)Rh(C_3H_6I). An irreversible reduction of (TPP)Rh(C_3H_6I) occurs at E_p = −1.37 V. This process is coupled with a reversible wave at $E_{1/2}$ = −1.84 V and an irreversible reoxidation wave at −0.20 V. There is also an additional oxidation wave at E_p = 0.35 V vs SCE. This process is due to the oxidation of I^-. This was confirmed by independent experiments with TBA^+I^- and a comparison with literature values for the oxidation of iodide in nonaqueous media.[2,12]

The formation of [(TPP)Rh]$_2$ upon reduction of (TPP)Rh(C_3H_6I) demonstrates cleavage of the Rh–carbon bond, but low-temperature electrochemical data suggest that [(TPP)Rh(C_3H_6I)]$^-$ can be stabilized and further reduced near −1.8 V. However, loss of $(C_3H_6I)^-$ occurs at room temperature, and the

(12) Bard, A. J.; Merz, A. *J. Am. Chem. Soc.* **1979**, *101*, 2959 and references therein.

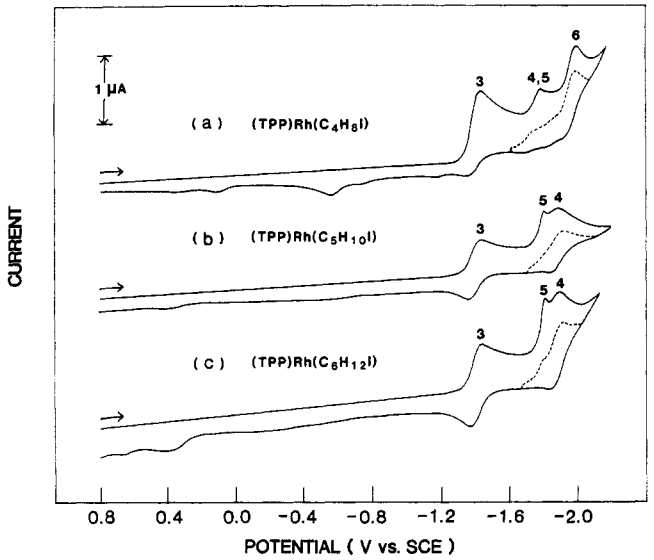

Figure 7. Cyclic voltammograms of (a) (TPP)Rh(C_4H_8I), (b) (TPP)-Rh($C_5H_{10}I$), and (c) (TPP)Rh($C_6H_{12}I$) in THF containing 0.2 M TBAP at a scan rate of 0.1 V/s: (—) first scan; (--) second scan.

second electron in the overall two-electron reduction of (TPP)-Rh(C_3H_6I) can be added to either $(C_3H_6I)^-$ or its decomposition products.

The effect of temperature on the cyclic voltammogram of (TPP)Rh(C_3H_6I) is shown in Figure 6 and demonstrates that an ECE mechanism occurs for either the first or the second process depending upon temperature. The room-temperature cyclic voltammogram of (TPP)Rh(C_3H_6I) in THF (Figure 6a) suggests a similar room-temperature mechanism in THF and PhCN. However, as the temperature is reduced, the rate of the chemical reaction following the initial reduction is slowed down. At −70 °C the first reduction (wave 3, Figure 6c) becomes reversible and occurs at $E_{1/2}$ = −1.43 V. No reduction or oxidation processes associated with $[(TPP)Rh]_2$ are observed at this temperature.

At −70 °C the second reduction process at −1.88 V (wave 5, Figure 6c) is then due to a further reduction of electrogenerated $[(TPP)Rh(C_3H_6I)]^-$. This reduction is irreversible in that the ratio of the anodic to cathodic peak current is no longer equal to unity. The peak current of the cathodic process is approximately twice that of the initial one-electron transfer on the first potential sweep, and the values of E_{pc} and E_{pa} are −1.88 and −1.84 V, respectively, at 100 mV/s. However, if the potential is scanned a second time, a reversible process ($i_{pc} = i_{pa}$) occurs at $E_{1/2}$ = −1.86 V. This process is labelled as wave 4 and is shown by the dashed line in Figure 6c. The maximum current of wave 4 is approximately the same height as the initial one-electron reduction at −70 °C (wave 3). This behavior suggests an ECE type mechanism at low temperature where the two electron transfers occur at or near −1.86 V.

The first reduction of (TPP)Rh(C_3H_6I) appears to be reversible at low temperatures, even after scanning past the second irreversible process. However, a chemical reaction follows the second reduction of (TPP)Rh(C_3H_6I) and results in a species that has reversible processes at $E_{1/2}$ = −1.43 and −1.86 V. One species with this electrochemical behavior is (TPP)Rh(R), as indicated by the scheme in Figure 3. This implies a loss of I^- from $[(TPP)Rh(C_3H_6I)]^{2-}$ in a reaction that is initiated by an electrochemical process. However, the exact nature of the R group of the electrogenerated species is unknown and the chemical reaction may involve more than loss of I^-. Similar voltammetric behavior is observed for complexes in the (TPP)Rh($C_nH_{2n}I$) and (TPP)Rh($C_nH_{2n}Br$) series.

Irreversible first reductions are obtained for (TPP)Rh(RX), where RX = $C_nH_{2n}I$ (n = 3–6). However, as the chain length of RX is increased from n = 3 to n = 6, the loss of RX^- following the initial one-electron reduction becomes kinetically very slow so that for n = 5 or 6 this reaction no longer has a significant influence on the cyclic voltammetry. The effect of chain length is illustrated by the cyclic voltammograms in Figure 7. The cyclic voltammogram of (TPP)Rh($C_6H_{12}I$) at room temperature (Figure 7c) is similar to that of (TPP)Rh(C_3H_6I) at −40 °C (Figure 6b). The loss of I^- from the doubly reduced (TPP)Rh($C_6H_{12}I$) with generation of a $[(TPP)Rh(R)]^-$ complex is proposed to be the primary reaction pathway on the cyclic voltammetry time scale. At −70 °C, each (TPP)Rh($C_nH_{2n}I$) complex has the same reductive behavior.

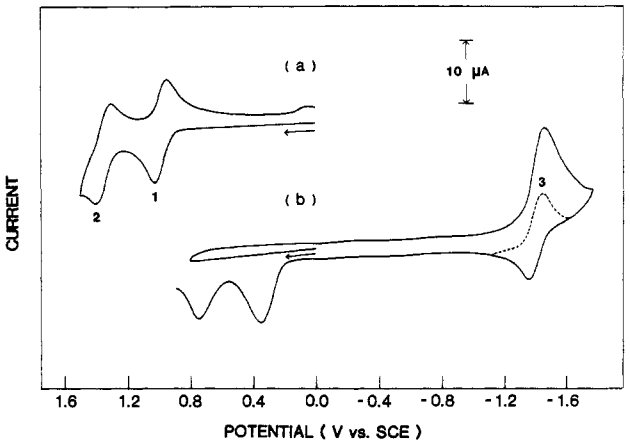

Figure 8. Thin-layer cyclic voltammogram for the (a) oxidation and (b) reduction of (TPP)Rh($C_6H_{12}I$) in PhCN containing 0.2 M TBAP: (—) first scan; (--) second scan.

Figure 8 shows a thin-layer cyclic voltammogram of (TPP)-Rh($C_6H_{12}I$) in PhCN. On this time scale, $[(TPP)Rh(C_6H_{12}I)]^-$ reacts chemically and the loss of I^- is observed. Two reversible one-electron oxidations (waves 1 and 2, Figure 8a) are observed at $E_{1/2}$ = 0.99 and 1.35 V when the potential is scanned in a positive direction. Figure 8b shows the reduction of this species on both the initial scan (solid line, Figure 8b) and the second scan (dashed line, Figure 8b). The data suggest an initial two-electron reduction of (TPP)Rh($C_6H_{12}I$). The value of i_{pc} is approximately twice i_{pa} for reoxidation of this complex, but additional sweeps give a reversible wave (wave 3, Figure 8b) with $i_{pc} = i_{pa}$.

Formation of I^- upon reduction of (TPP)Rh($C_6H_{12}I$) is indicated by the oxidation waves at E_p = 0.35 and 0.75 V. Thin-layer coulometric reduction of (TPP)Rh($C_6H_{12}I$) at −1.70 V gives a value of n = 2.1 ± 0.2, while reoxidation at 0.00 V gives n = 1.0 ± 0.2. This coulometric data is consistent with a loss of I^- from $[(TPP)Rh(C_6H_{12}I)]^-$. Hence, wave 3 in Figure 8b is assigned as the reversible reduction of the electrogenerated (TPP)Rh(R) complex. Similar behavior is observed on the thin-layer cyclic voltammetric time scale for (TPP)Rh($C_5H_{10}I$) and hence demonstrates a similar chemical reaction following reduction.

The thin-layer cyclic voltammogram of (TPP)Rh(C_4H_8I) is substantially different from conventional cyclic voltammograms of this compound. The initial reduction is irreversible in the thin-layer experiment indicating a chemical reaction on this time scale. Two new reversible waves are observed at $E_{1/2}$ = +0.10 and −0.59 V. The identity of the generated species is not known, but loss of I^- from (TPP)RH(C_4H_8I) also occurs as indicated by the observation of an irreversible wave at E_p = 0.35 and 0.75 V.

The spectroelectrochemically monitored reduction of (TPP)-Rh(C_3H_6I) demonstrates that formation of $[(TPP)Rh(C_3H_6I)]^-$ (process 3) at −1.65 V is followed by cleavage of the rhodium–carbon bond and generation of $[(TPP)Rh]_2$. The initial species is characterized by bands at 411 and 524 nm. After reduction by two electrons, the Soret band is shifted to 403 nm while a new band is observed at 496 nm as $[(TPP)Rh]_2$ is formed.[1] The initial reduction of (TPP)Rh($C_5H_{10}I$) and (TPP)Rh($C_6H_{12}I$) appear to be ring centered, and in the case of (TPP)Rh($C_6H_{12}I$) the spectrum is characterized by bands at 403, 497, 580, and 700 nm.

Reduction of (TPP)Rh($C_nH_{2n}Br$). Cyclic voltammograms for (TPP)Rh($C_nH_{2n}Br$) (n = 3–5) in THF are shown in Figure 9 and indicate that the chemical reactions following the intiial one-electron transfer are slower than the chemical reactions observed

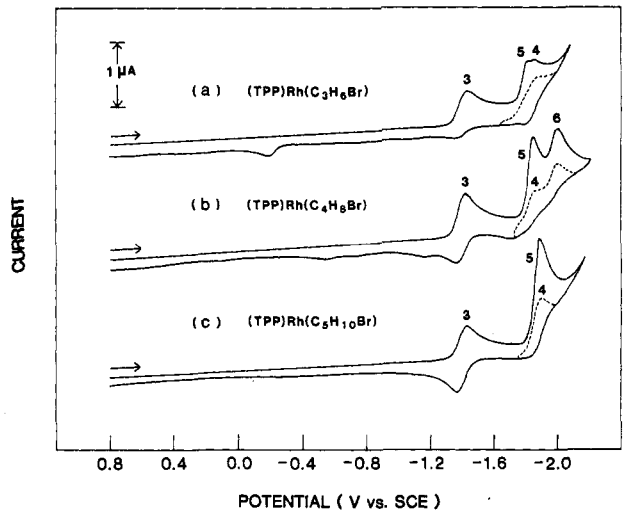

Figure 9. Cyclic voltammograms of (a) (TPP)Rh(C_3H_6Br), (b) (TPP)Rh(C_4H_8Br) and (c) (TPP)Rh($C_5H_{10}Br$) in THF containing 0.2 M TBAP at a scan rate of 0.1 V/s: (—) first scan; (- -) second scan.

for compounds in the (TPP)Rh($C_nH_{2n}I$) series. The first reduction of (TPP)Rh(C_3H_6Br) (wave 3, Figure 9a) is not totally reversible on the cyclic voltammetric time scale, but a further reduction of [(TPP)Rh(C_3H_6Br)]$^-$ (waves 4 and 5, Figure 9a) can be observed. Reduction of [(TPP)Rh(C_3H_6Br) results in cleavage of the rhodium–carbon bond and formation of [(TPP)Rh]$_2$. The mechanism for dimer formation is similar to the one suggested for (TPP)Rh(C_3H_6I) and is supported by thin-layer cyclic voltammetric experiments that show an irreversible reduction at $E_p = -1.39$ V in THF containing 0.2 M TBAP. Thin-layer coulometric values of $n = 2.6 \pm 0.2$ are observed for reduction of (TPP)Rh(C_3H_6Br) at −1.62 V in THF.

The primary difference between (TPP)Rh(C_3H_6Br) and (TPP)Rh(C_3H_6I) is that the chemical reaction following the initial reduction is slower for (TPP)Rh(C_3H_6Br). Hence, room-temperature cyclic voltammograms of (TPP)Rh(C_3H_6Br) resemble those of (TPP)Rh(C_3H_6I) at reduced temperatures. In addition, the cyclic voltammogram of (TPP)Rh(C_3H_6Br) at −70 °C is characterized by two reversible reductions and is basically the same as that of (TPP)Rh(C_3H_6Cl) at room temperature. This indicates that the chemical reaction following reduction of (TPP)Rh(C_3H_6Br) is not significant at low temperature on the cyclic voltammetric time scale.

The first reduction of (TPP)Rh(C_4H_8Br) (wave 3, Figure 9b) is nearly reversible, and a second and third reduction are also observed. (waves 4 and 5, Figure 9b). An additional reduction (wave 6) is observed for this species at $E_p = -2.01$ V and is assigned as reduction of a decomposition product. This assignment is based on low-temperature cyclic voltammetric studies of (TPP)Rh(C_4H_8Br). At −70 °C, wave 6 is decreased in current relative to waves 3, 4, and 5, and the overall appearance of the cyclic voltammogram is similar to that of (TPP)Rh(C_3H_6I) at −70 °C. Thin-layer cyclic voltammetric studies on (TPP)Rh(C_4H_8Br) suggest that reduction of this species results in loss of both Br^- and $C_4H_9Br^-$ since [(TPP)Rh]$_2$ and a (TPP)Rh(R) species are observed.

The cyclic voltammogram of (TPP)Rh($C_5H_{10}Br$) is shown in Figure 9c and is similar to the voltammogram of (TPP)Rh($C_6H_{12}I$). Loss of Br^- and possible further reaction of [(TPP)Rh($C_5H_{10}Br$)]$^{2-}$ with generation of a [(TPP)Rh(R)]$^-$ complex is observed on the cyclic voltammetric time scale. The thin-layer cyclic voltammogram of (TPP)Rh($C_5H_{10}Br$) is very similar to that of (TPP)Rh($C_5H_{10}I$) or (TPP)Rh($C_6H_{12}I$), but differs in that Br^- rather than I^- oxidation is observed at anodic potentials. Hence, loss of Br^- from the singly reduced species is proposed to occur on this time scale.

Spectroelectrochemical experiments also demonstrate that the rhodium–carbon bond is cleaved following an initial ring-centered reduction of (TPP)Rh(C_3H_6Br). For example, the original UV–visible bands of (TPP)Rh(C_3H_6Br) decrease in intensity upon reduction at −1.62 V while new bands are observed at 403, 497, and 516 nm. Hence, formation of [(TPP)Rh]$_2$ is observed when the potential is held at −1.62 V.

In general, irreversible reductions at the bound RX ligand are observed for (TPP)Rh(RX), where RX = $C_nH_{2n}I$ or $C_nH_{2n}Br$. The value of E_{pc} for this reduction is dependent upon the chain length and the halide of the R group and follows the trend predicted for reduction of alkyl halides.[4,5] This provides further evidence for a reduction and chemical reaction of the R group. Reduction of the bound RX occurs at $E_{1/2}$ values significantly less negative than those for reduction of free RX or RX_2 under the same solution conditions.

In summary, we have demonstrated that the R group in (TPP)Rh(R) can direct the electrochemical behavior observed for these compounds. This is perhaps unexpected since the initial reduction of (TPP)Rh(R) occurs at the porphyrin π ring system and $E_{1/2}$ for (TPP)Rh(R) and (TPP)Rh(RX) reduction varies within a narrow potential range. Hence, any changes in reactivity are not due to an inductive effect of the R group.

Acknowledgment. The support of the National Science Foundation (Grant No. CHE-8515411) is gratefully acknowledged.

Registry No. (TPP)Rh(CH_3), 103562-25-0; [(TPP)Rh(CH_3)]$^+$, 110316-76-2; [(TPP)Rh(CH_3)]$^{2+}$, 110316-80-8; (TPP)Rh(C_2H_5), 103533-58-0; [(TPP)Rh(C_2H_5)]$^+$, 110316-77-3; [(TPP)Rh(C_2H_5)]$^{2+}$, 110316-81-9; (TPP)Rh(C_3H_7), 106161-22-2; (TPP)Rh(C_4H_9), 106161-23-3; (TPP)Rh(C_5H_{11}), 106161-24-4; [(TPP)Rh(C_5H_{11})]$^+$, 110316-78-4; [(TPP)Rh(C_5H_{11})]$^{2+}$, 110316-82-0; (TPP)Rh(C_6H_{13}), 106799-98-8; (TPP)Rh(C_6H_5), 110316-66-0; (TPP)Rh(C_3H_6Cl), 110316-67-1; (TPP)Rh(C_3H_6Br), 110316-69-3; [(TPP)Rh(C_3H_6I)]$^-$, 110316-84-2; (TPP)Rh(C_3H_6I), 110316-72-8; [(TPP)Rh(C_3H_6I)]$^+$, 110316-79-5; [(TPP)Rh(C_3H_6I)]$^{2+}$, 110316-83-1; (TPP)Rh(C_4H_8Cl), 110330-24-0; (TPP)Rh(C_4H_8Br), 110316-70-6; (TPP)Rh(C_4H_8I), 110316-73-9; (TPP)Rh($C_5H_{10}Cl$), 110316-68-2; (TPP)Rh($C_5H_{10}Br$), 110316-71-7; (TPP)Rh($C_5H_{10}I$), 110316-74-0; [(TPP)Rh($C_6H_{12}I$)]$^-$, 110316-85-3; (TPP)Rh($C_6H_{12}I$), 110316-75-1; [(TPP)Rh]$_2$, 88083-37-8; Rh, 7440-16-6.